physica **pss** status solidi **a**
www.pss-a.com
applications and materials science

Contactless electrical defect characterization in semiconductors by microwave detected photo induced current transient spectroscopy (MD-PICTS) and microwave detected photoconductivity (MDP)

Bastian Berger[1], Nadine Schüler[2], Sabrina Anger[2], Bianca Gründig-Wendrock[3], Jürgen R. Niklas[2], and Kay Dornich*,[2]

[1] Institute of Theoretical Physics, TU Bergakademie Freiberg, Leipziger Straße, 09596 Freiberg, Germany
[2] Freiberg Instruments GmbH, Am St. Niclas Schacht 13, 09599 Freiberg, Germany
[3] SolarWorld Innovations GmbH, Berthelsdorfer Straße 111a, 09599 Freiberg, Germany

* Corresponding author: e-mail dornich@freiberginstruments.com, Phone: +49 3731 41 95 410, Fax: +49 3731 41 95 414

The contactless electrical characterization techniques MDP and MD-PICTS will be presented in this paper. Both methods are predestined for defect investigation in a variety of semi-conductors. Due to a so far not reached sensitivity, major advantages of MDP are its high spatial resolution and its measurement speed, which allows for two dimensional inline measurements at production speed. Furthermore a versatile numerical tool for simulations of electrical properties of a semiconductor as a function of defect parameters was developed. MD-PICTS is a contactless temperature dependent measurement which allows the determination of activation energies of trap levels in the material. To demonstrate the abilities of both methods, measurements conducted at different semiconductor materials, *e.g.* silicon, silicon carbide, gallium arsenide and indium phosphide, will be presented exemplarily.

1 Introduction and motivation In photovoltaic as well as in microelectronic industry the goal is to drive costs down by bringing yields up at the same time. To reach this goal it is important to analyze the defects existing in the used semiconductor materials and their impact on the latter device performance. Therefore the two contactless electrical characterization methods MDP and MD-PICTS for defect investigation are presented and results at different semi-conductor materials are reviewed.

Due to the advanced microwave detection technique both methods have an advantage of sensitivity. As a consequence a high measurement speed is enabled. Mapping of 156 mm mc-Si wafer takes under a second [1]. The wide measurable injection range from 10^{10} to 10^{17} cm^{-3} is another benefit. Extraction of several defect parameters like the activation energy of the main recombination center from injection dependent investigations is possible. The high sensitivity is also used for measurements on lower qualitative materials or thin epitaxial layers on various substrates [2]. Using the varying penetration depth of light from different wavelength reveals even information about interface defects.

As one example the influence of metal contaminations as iron and chromium in silicon, diffusing into the material during the melting process and reducing the efficiency of solar cells and causing breakdowns of devices, is widely discussed in literature [3], as well as lifetime degradation caused by BO_2 [4]. MDP is a suitable tool for high resolution mappings of the density of iron as well as chromium and boron–oxygen complexes. Furthermore due to high sensitivity and steady state measurements iron mapping in multicrystalline silicon bricks is even possible as inline measurement, revealing the concentration of all electrically active Fe.

MD-PICTS is an advancement of conventional photo induced current transient spectroscopy (PICTS) without the necessity of contacting the samples and with a higher sensitivity, opening new fields of applications on a variety of semiconductors revealing so far not accessible defect information. The technique is sensitive to defects acting as carrier traps while the DLTS method gives more information about the dominating recombination center in the material.

To achieve a better understanding of measured results a versatile numerical simulation tool was developed. It strictly starts from first principles rather than relying, *e.g.* on SRH formalism and similar approximations. Application of this tool makes it possible to determine the impact of certain defect properties on important material parameters as minority carrier lifetime, photoconductivity or diffusion length. Thus it is used to simulate MD-PICTS and MDP measurements by taking different defects into account.

2 Experimental details

2.1 Microwave detected photoconductivity
The novel method MDP is well suited for both, defect investigation by, *e.g.* injection dependent minority carrier lifetime measurements, as well as mapping of wafers or even bricks for inline metrology. Its major advantage is the combination of sensitivity, resolution and speed, giving MDP the flexibility for a wide variety of different applications.

The photoconductivity, which is closely related to the diffusion length, is measured by microwave absorption in a resonant microwave cavity, during and after the excitation with a rectangular laser pulse. Figure 1 shows the layout of the MDP and MD-PICTS measurement setup. The sample is situated just outside the microwave cavity and is part of the measurement system. Thus, the complex dielectric constant of the sample influences the resonant frequency and the loss properties of the cavity. The microwave absorption by excess charge carriers is detected. The sample is placed on an *x–y*

Figure 1 (online color at: www.pss-a.com) Scheme of MDP measurement setup.

table, allowing theoretically every sample size and to move the sample in the *x–y* plane.

The high detection sensitivity enabled by this technique allows for injection dependent measurement over more than eight orders of magnitude depending on material under investigation with unlimited duration facilitating experiments in a non-equilibrium or steady state regime. Another major advantage of MDP is the ability to measure photoconductivity and minority carrier lifetime simultaneously. The minority carrier lifetime τ can be extracted from the semi logarithmic decay and the photoconductivity equals the signal height at steady state. Accordingly a variety of information can be gained from each measurement, like diffusion length, mobility, and even trapping dynamics.

2.2 Microwave detected photo induced current transient spectroscopy
For defect investigation on semiconductors deep level transient spectroscopy (DLTS) [5] and the photo induced current transient spectroscopy (PICTS) [6] are established techniques for more than 20 years. Both differ in their excitation mechanism and detection. While DLTS uses capacitive determination of excite charge reversal of defects caused by voltage pulses, PICTS measures the photoconductivity due to local irradiation with laser light. Therefore contacting of samples is required for both methods. Microwave detected PICTS is an advancement of the conventional method, working contactless and therefore non-destructive.

To measure temperature dependent MD-PICTS, the MDP equipment shown in Fig. 1 is applied, with an additional cryostat for the sample. The setup allows for spatially resolved measurements.

The method [7, 8] is based on the non-destructive investigation of photoconductivity signals by microwave absorption. Through pulsed light excitation provided by a laser excess carriers are generated in the material. According to intended investigation, wavelengths from UV- until the IR-range are applied, allowing for depth profiling as well as defect specific excitation with sub-band-gap wavelength. The light excitation causes a local rise of conductivity to a level dependent on the generation and recombination processes as well as on trapping and reemission dynamics (time interval 1 in Fig. 2). After the laser pulse is turned off the signal decreases rapidly caused by the fast recombination of the generated excess carriers (time interval 2). The slope of the so-called transient depends on the recombination rate. This initial fast decay is followed by a slower decreasing part due to the reemission of trapped carriers into the associated band (time interval 3). Appropriate analysis leads to the extraction of defect parameters, *e.g.* the activation energy. After the photoexcitation, recombination and trapping of charge carriers the typical photoconductivity transient based on the thermal excited emission follows:

$$\Delta\sigma_{\text{Transient}} = q\mu\Delta n = q\mu n_{T_0}\tau_n \cdot e^{-e_{n_T}^t t}, \tag{1}$$
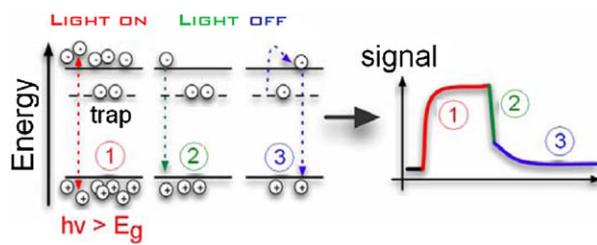
Figure 2 (online color at: www.pss-a.com) Physical processes and their corresponding signal parts in MD-PICTS: (1) generation and trapping of carriers, (2) fast recombination process, (3) thermal reemission of trapped carriers [8].

n_{T_0} corresponds to the initial density of carriers trapped by a distinct defect, $e^t_{n_T}$ symbolizes the thermal excited emission rate of this trap and t is the time after the termination of the photo pulse. From $e^t_{n_T}$ the activation energy of a trap can be calculated using the relation

$$e^t_{n_T} = AT^2 \cdot e^{-\frac{E_A}{kT}}, \tag{2}$$

where A is a material constant.

For analysis the so-called two-gate technique according to DLTS is used leading to a similar defect spectra. MD-PICTS can be applied from semi-insulating samples to conductive ones. This opens characterization possibilities even on silicon which has not been possible with conventional PICTS. With the used cooling system the temperature range for MD-PICTS measurements is 80 to 500 K. Cooling down to 4 K is possible, but investigations suggest that liquid nitrogen temperature is sufficient for most defects. The filling pulse differs depending on the sample's properties between 10 and 1000 µs.

2.3 Materials and samples To show the potential of the contactless electrical characterization methods MDP and MD-PICTS, results from analysis of several semiconductor materials will be reviewed.

Shown MDP measurements for defect investigation are on passivated mc- and Cz-Si samples. For defect investigation by MDP-PICTS following samples were available: high quality 6 inch electronic grade p-doped mono-crystalline silicon with a specific resistivity around 12 Ω cm; solar grade multi-crystalline p-type silicon from different parts of a brick; single-crystalline GaAs wafer from different preparations [vertical gradient freeze (VGF) and liquid encapsulated Czochralski (LEC)]; InP samples from Fe-doped crystals with a resistivity between 0.01 and 2×10^8 Ω cm and semi-insulating 6H-SiC wafer grown by HTCVD with resistivities exceeding 2×10^9 Ω cm.

3 Simulations During the development and application of MDP and MD-PICTS it became clear that the obtained results are often not describable by simple defect models. The widely used SRH-Theory is only applicable if no trap influence is assumed, which is invalid especially for low injection measurements at *e.g.*, mc-Si and MD-PICTS measurements in general, where this trap influence is investigated. This leads to the necessity of a new simulation tool without any approximations that is able to simulate injection and temperature dependent lifetimes as well as the trapping dynamics.

The numerical tool is based on a generalized rate equation system. The rate equations are used to describe the time dependent change of the carrier occupation of the bands ($\dot{n}, \dot{p}$) and defects ($\dot{n}_{Tj}$). All possible transitions between the defect levels in the forbidden gap and the bands of a semiconductor are described by transition rates.

A rate equation system is used, in which the only approximation is, that no direct interactions between defect levels are included [9].

$$\dot{n} = G^o_{BB} + G^{th}_{BB} + \sum_j (C_j - D_j) - U_{BB} - U_{Aug}, \tag{3}$$

$$\dot{p} = G^o_{BB} + G^{th}_{BB} + \sum_j (F_j - E_j) - U_{BB} - U_{Aug}, \tag{4}$$

$$\dot{n}_{Tj} = D_j + E_j - C_j - F_j. \tag{5}$$

Based on the simulated time dependent carrier concentrations, the photoconductivity can be calculated using the mobility model of Dorkel and Leturcq [10]. The minority carrier lifetime finally can be extracted from the simulated transient decay of the photoconductivity after G_{opt} is set to zero or can be determined from the photoconductivity value, if a quasi steady state approach is used. Consequently, the technique which is used to evaluate the lifetime values from the simulated data is strictly based on the used measurement technique and thus is correlated to the lifetime evaluation technique which is experimentally applied. Therefore a very good agreement between simulated values and measurement results is guaranteed. More details and a demonstration of the abilities of this simulation tool can be found in Ref. [11].

4 Experimental results and discussion
4.1 Microwave detected photoconductivity Some of the most detrimental defects in silicon are traps in general, iron, boron–oxygen complexes and chromium. All these defects have been investigated extensively in the last decades. With MDP it is possible to investigate these defects with a high resolution and by injection dependent lifetime measurements over a wide range of injections. Examples at passivated crystalline silicon wafers are presented.

With the ability of MDP to measure the lifetime and photoconductivity simultaneously, it is possible to estimate the trap density in mc-Si by the slightly modified model of Hornbeck and Haynes [12]. This model includes only one trap level, so that the determined trap density is only an estimation. By fitting the photoconductivity as a function of the optical generation rate, the trap density and activation energy can be determined. The following formula is used for

the fitting:

$$\Delta\sigma = e\left[\Delta n\left(\mu_n + \mu_p\right) + \mu_p \frac{\Delta n \cdot N_T}{\Delta n + N_C \cdot \exp\left(\frac{-E_a}{kT}\right)_T}\right] \quad (6)$$

Figure 3 shows an exemplary photoconductivity measurement at a mc-Si wafer, the fit-curve and the corresponding measured apparent lifetime.

By MD-PICTS measurements it is possible to separate different trap levels, but no information about the trap density is provided. By applying both methods a comprehensive study about traps in a sample can be conducted.

The iron detection by lifetime measurements is widely spread in the photovoltaic industry. The FeB pairs are dissociated by irradiating the sample with light and from the deviation between the measured lifetime before and after the dissociation the iron concentration can be determined via the following formula:

$$[\text{Fe}] = C_{\text{Fe}}\left(\frac{1}{\tau_{\text{after}}} - \frac{1}{\tau_{\text{before}}}\right). \quad (7)$$

The accuracy of this determination depends strongly on the use of an accurate calibration factor C_{Fe}, which depends on the injection, doping and trap density. By using the rate equation simulations it is possible to simulate the correct calibration factor for every possible measurement condition [13]. Figure 4 shows an exemplary iron map of a mc-Si wafer with a resolution of 0.5 mm.

One difficulty of the iron detection is the separation from other defects, which also react on the irradiation with light, e.g. BO_2. With several annealing steps and repeated irradiation, it is possible to separate FeB and BO_2, since both defects differ in their association time constants and response to elevated temperatures. For the BO_2 determination Eq. (7) is also used, only with the calibration factor for BO_2 (C_{BO2}), which is simulated with the according defect parameters [14]. Since especially the carrier cross sections are not known exactly for BO_2, only a relative concentration can be measured. Figure 5 displays the maps of the relative
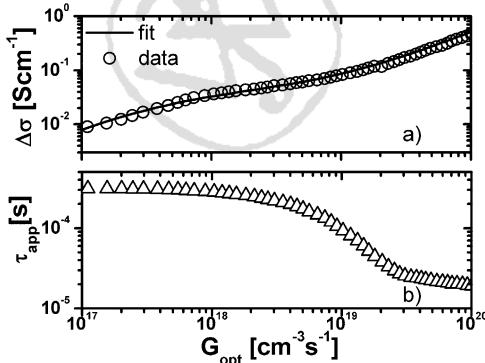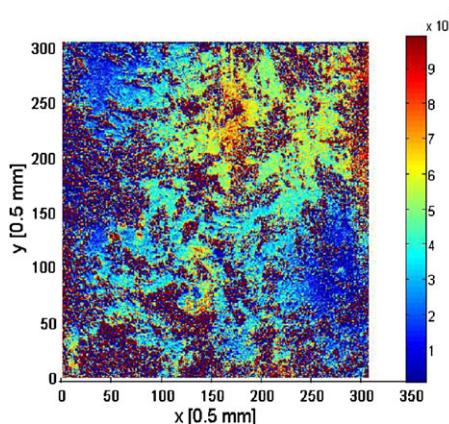

Figure 4 (online color at: www.pss-a.com) Exemplary iron map of a SiN$_x$ passivated mc-Si wafer with a resolution of 0.5 mm.

BO_2 and Fe concentration of an oxide passivated Cz-Si wafer. With these measurements typical differences in the distribution of both defects become obvious. Iron is concentrated at the edge of the sample, whereas BO_2 is
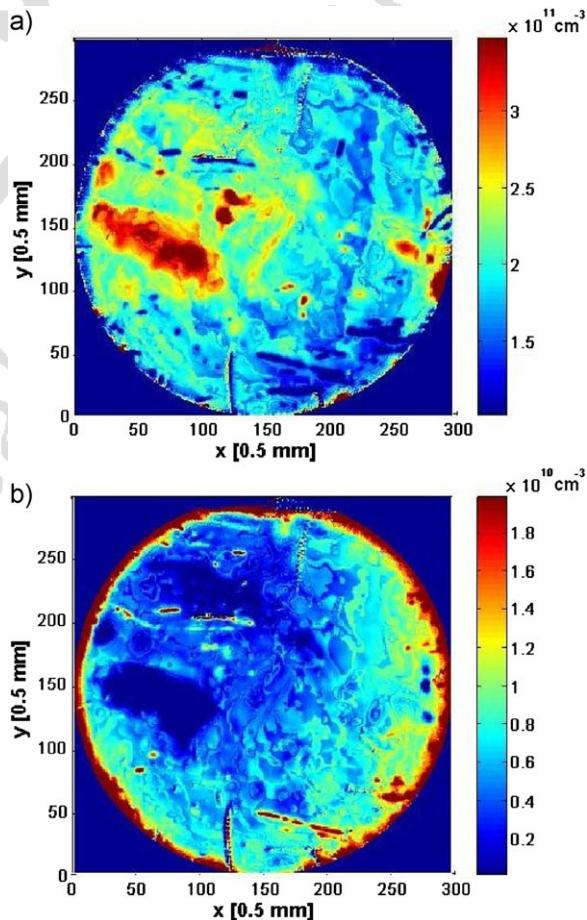

Figure 3 Measured photoconductivity and fit curve versus G_{opt} (a); apparent lifetime versus G_{opt} (b); determined trap parameter: $N_T = 8 \times 10^{14}\,\text{cm}^{-3}$, $E_A = 0.387\,\text{eV}$ [13].

Figure 5 (online color at: www.pss-a.com) Relative BO_2 concentration (a) and Fe concentration (b) of an oxide passivated Cz-Si wafer.
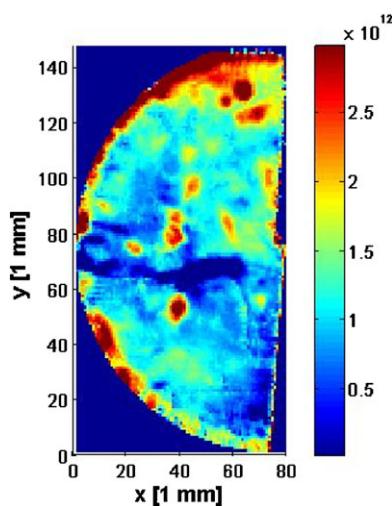
Figure 6 (online color at: www.pss-a.com) Exemplary map of the relative chromium concentration of an intentionally doped Cz-wafer.

Figure 7 Spectra of temperature treated electronic grade p-doped silicon [16].

distributed in high concentrated regions in the middle of the wafer. As mentioned above chromium is also an effective recombination center in silicon. Similar to iron it occurs as CrB in boron doped silicon and can be dissociated to Cr_i and B by annealing the sample for 30 min at 250 °C. For the chromium determination Eq. (7) is also applied with a calibration factor C_{Cr}. To determine the injection dependent calibration factor C_{Cr} the defect parameters from [15] were used. Note that similar to BO_2 defect parameters of CrB and Cr_i are not well known so far. That is why only the relative density is determined. An exemplary map of the relative chromium concentration of an intentionally chromium doped Cz-wafer is shown in Fig. 6.

By spatially resolved MD-PICTS measurements, it is possible to investigate the defect distribution of different regions of the here presented samples, in order to learn more about the correlation of *e.g.*, BO_2 and thermal donors (TDs). An example of an investigation of TDs in silicon by MD-PICTS is presented in the next section.

4.2 Microwave detected photo-induced current transient spectroscopy In contrast to DLTS a direct detection of metal contaminations like iron and chromium in silicon with PICTS is so far not successful because these defects are mostly acting as the main recombination centers. But by improving the sensitivity of a microwave detection system by several orders of magnitude the visualization of so far non-detectable defects in electronic grade silicon was achieved. One example is the electrical investigation of the well-known TD in electronic grade p-doped silicon [16]. It is not detectable with DLTS because of the position of the Fermi level. The MD-PICTS spectra in Fig. 7 shows two defect levels called PTD and PD. Following their evolution during thermal treatment suggests that the PTD peak refers to the TDs in silicon. After annealing for 40 min at 650 °C the emission maximum shifts more than 40 K to lower
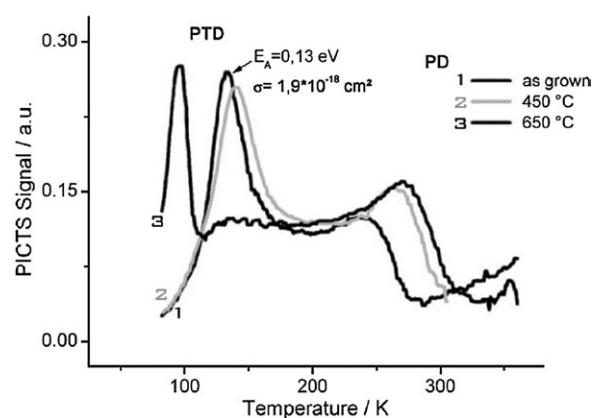
temperatures and is now located at 96 K (previously 133 K in the as-grown state and 140 K in the 450 °C treated sample). This is due to the change in capture cross section from $\sigma = 2 \times 10^{-18} \, cm^{-2}$ in the as-grown material to $\sigma = 2 \times 10^{-15} \, cm^{-2}$ in the 650 °C treated sample. The activation energy shifts only slightly from $E_A = 0.13$ to $E_A = 0.11 \, eV$. The change of position is believed to be caused by the transformation of an electrically active TD state into an electrically inactive trap state at temperatures above 600 °C [17]. At higher temperatures above 900 °C the intensity of the defect peak drops rapidly suggesting the dissociation of this defect level. A second defect level with $E_A = 0.26 \, eV$ in as-grown samples at 242 K can be observed. It is caused by defects in the vicinity of dislocations. Correlations with PL measurements carry this assumption.

With MDP and MD-PICTS it is possible to obtain a deeper understanding of the observed sharp transition in the electrical properties of wafers prepared from different parts of a silicon brick [18]. The PTD and PD peaks known from electronic grade p-doped silicon and additional peaks are found by investigations of solar grade silicon samples (Fig. 8). P4 with an activation energy of 0.09 eV is only observable in the bottom part. Because of this low activation energy, the large width of the peak and the position of the corresponding wafer in the silicon brick it may be ascribed to a defect cluster containing nitrogen. P3, whose activation energy cannot be deduced, may have its origin in a cluster of bulk defects, because different surface treatments do not influence the peak. The appearance of all defect peaks differs from the associated brick position. Mapping the samples with MDP shows corresponding changes in lifetime, diffusion length, and photoconductivity.

Beside investigations on silicon the new method for contactless electrical defect characterization was applied on gallium arsenide. MD-PICTS spectra show that a high density of the so-called EL5-defect in cell interior regions is responsible for dark areas of smaller lifetimes in MDP mappings [7]. In contrast to other techniques MD-PICTS can detect signals even from thin surface regions (0.3 μm) of SI GaAs samples and is therefore able to analyze, *e.g.*
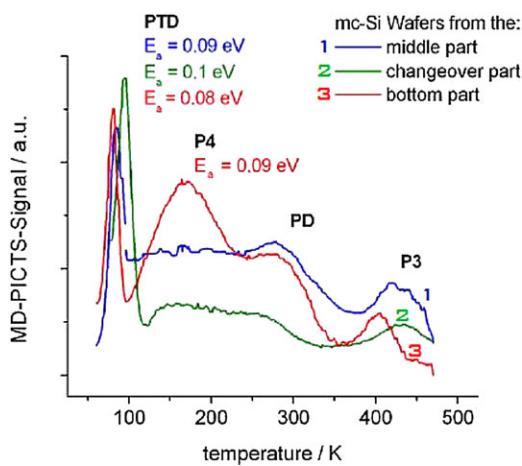
Figure 8 (online color at: www.pss-a.com) MD-PICTS spectra of solar grade p-doped silicon samples from different brick heights [18].

influences of surface treatments. Figure 9 shows the defect peak of the well-known EL2 defect in samples with different acceptor concentrations [19]. The activation energy varies between 0.55 and 0.73 eV which is in agreement with data from other groups [20, 21]. Conspicuous is the occurrence of the defect peak in positive and negative form.

The explanation of the negative PICTS peak effect is based on the system of rate equations from Section 3, which calculates the carrier concentration of the involved energy levels by taking all participating generation and recombination processes as well as trapping and emission events during and after the photo excitation into account. Therefore photoconductivity signals, as they are measured as a result of the photo generation of carriers, can be simulated for different temperatures, if an appropriate mobility is taken into account. The consideration of the relevant donor and acceptor concentrations along with the concentration of the EL2 defect finally allows for the theoretical reproduction of
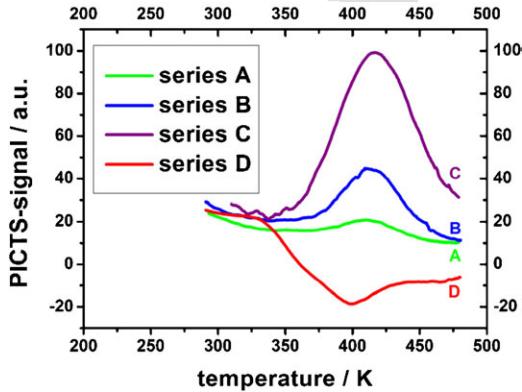
experimental results. The latter show a dependence of the height of the EL2-related PICTS peak on the acceptor concentration in the material thus being associated with the Fermi level position. To briefly summarize the theoretical investigations it can be said that the fast recombination and trapping dynamics in the III-V-compound semiconductor GaAs lead to a drop of the electron concentration below the equilibrium value after the excitation is switched off, while the hole concentration shows a positive decay behavior. The amount of electrons that can be trapped and thus the ratio of the concentrations of the two types of excess carriers remaining in the bands ($\Delta n/\Delta p$) are determined by the initial occupation of the electron trap (EL2) and therefore by the position of the Fermi level. The resulting photoconductivity signal

$$\Delta \sigma = \mathrm{e} \cdot (\mu n \Delta n + \mu p \Delta p) \qquad (8)$$

is consequently controlled by the behavior of the dominant current fraction, thus also considering the large difference of the carrier mobility values for GaAs ($\mu n/\mu p \approx 20$). That means a positive decay behavior of the photoconductivity signal is only observable, if the excess hole concentration remarkably exceeds the excess electron concentration leading to signal

$$\mu n \Delta n < \mu p \Delta p. \qquad (9)$$

This is the case for a Fermi level leaving most of the EL2 defect levels unoccupied [9].

Investigations on indium phosphide show that the defect content changes during annealing processes, which may also have an impact on the distribution of electrical properties. Whereas the defect content of as-grown samples depends on their position in the crystal, an equivalent set of defect levels is prominent in wafer-annealed samples [22]. Figure 10 shows a comparison of Fe-doped SI-InP samples from different crystal positions. They differ in their characteristic

Figure 9 (online color at: www.pss-a.com) Detection of the EL2d-efect in SI GaAs samples with different acceptor concentrations by HT-MD-PICTS. Peak height and sign correlate to the acceptor concentrations [19]. Samples from series D were undoped, acceptor concentration rising from A to C.
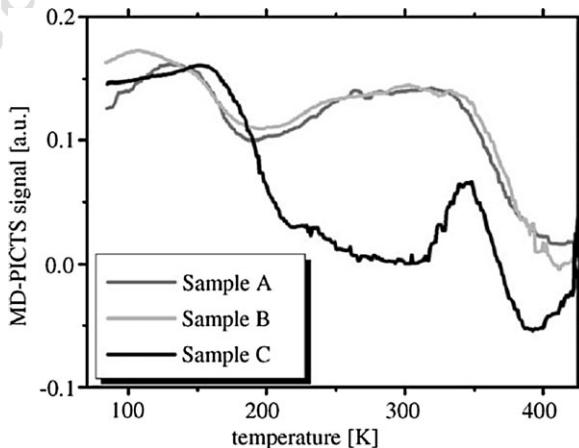

Figure 10 Comparison of MD-PICTS spectra of as-grown Fe-doped SI-InP samples from different crystal positions and thus different Fe-concentrations. The samples differ in their characteristic defect levels [22].
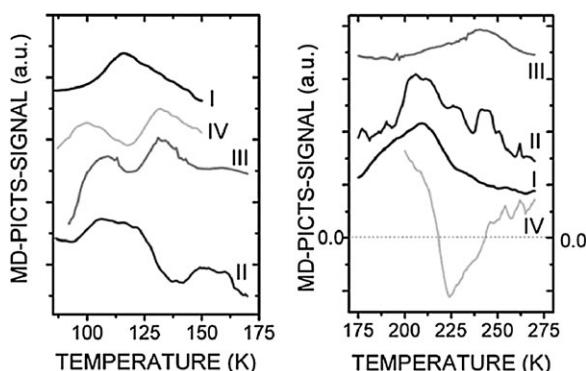
Figure 11 Comparison of MD-PICTS spectra of different SI-6H-SiC samples in different temperature ranges. Samples I–III were grown under same process conditions [8].

defect levels. Additional negative peaks occur in some samples for temperatures above 350 K with the amplitude increasing with the crystal length. The occurrence of peaks with different magnitude and sign in this temperature range is Fe-related. The negative peak is assigned to a transition of a hole leaving the Fe^{3+} level toward the valence band [23]. The observation of MD-PICTS signals of both signs in Fe-doped InP provided the first direct proof of iron acting as a recombination center in InP.

Analyses of semi-insulating 6H-SiC grown with a standard process and same process parameters show several differing shallow defect levels occurring in the low temperature range (Fig. 11). Additionally in samples grown under different C/Si-ratios different trap emission dynamics are obtained for higher temperatures, which are supposed to be due to different compensation effects [8]. The activation energies and capture cross sections of the defect peaks calculated from the spectra from Fig. 11 lie in the same range known from the literature [24–26]. They are traced back to omnipresent donor- and acceptor-like impurities and intrinsic defects.

5 Conclusion The presented experimental results show the potential of the new methods MDP and MD-PICTS for contactless electrical characterization of defects in several semiconducting materials. Both techniques use the sensitivity benefit of microwave detection leading to a high spatial resolution and measurement speed as well as the possibility to recognize defects which were not investigated yet. A cooperation of MDP and MC-PICTS, *e.g.* mapping of a sample and analysis of several areas differing in reported lifetime with MD-PICTS for defect recognition, leads to insights of the cause of different measurable effects. The introduced simulation tool helps to get a deeper understanding of the experimental data. To demonstrate the abilities of both methods, a range of previous results on defect characterization were reviewed in this paper.

By determination of a calibration factor depending on injection level, doping and trap density MDP is a useful technique to map the local iron concentration with a high

spatial resolution. Investigations on Cz-Si wafers show the typical differences in distribution of Fe_i and BO_2. While iron is concentrated at the edge of the sample, BO_2 is more distributed in the middle of the wafer.

With MD-PICTS experiments the visualization of so far non-detectable defects was achieved. One example is the investigation of the TD defect level in electronic grade p-doped silicon. This defect cannot be obtained with DLTS because of the position of the Fermi level. Samples from solar grade mc-Si show different defect levels due to their brick height. Comparison between MD-PICTS spectra and lifetime mappings with MDP on gallium arsenide wafers lead to the assumption that lifetime degradation of several areas is caused by the EL5 defect. The EL2 defect was also analyzed. The differentiation between the single ionized state $EL2^+$ from the $EL2^0$ is possible with the help of the signal sign. Investigations on Fe-doped indium phosphide gave the first direct proof that iron acts as recombination center in this material. In SI 6H-SiC the defect levels known from the literature were detected with similar activation energies and capture cross-sections. A deeper understanding about the appearance of PICTS-signals of different signs with simulations basing on a rate equation system has been accomplished.

References

[1] K. Dornich, N. Schüler, D. Mittelstraß, A. Krause, B. Gründig-Wendrock, K. Niemietz, and J. R. Niklas, Proceedings of the 24th European Photovoltaic Solar Energy Conference, Hamburg, Germany, 2009, pp. 1106–1108.

[2] K. Dornich, T. Hahn, and J. R. Niklas, Mater. Res. Symp. Proc. **864**, 549 (2005).

[3] A. A. Istratov, H. Hieslmair, and E. R. Weber, Appl. Phys. A **69**, 13 (1999).

[4] J. Schmidt and K. Bothe, Phys. Rev. B **69**, 024107 (2004).

[5] D. V. Lang, J. Appl. Phys. **45**, 3023 (1974).

[6] O. Yoshie and M. Kamihara, Jpn. J. Appl. Phys. **22**, 621 (1983).

[7] B. Gründig-Wendrock, M. Jurisch, and J. R. Niklas, Mater. Sci. Eng., B **91-92**, 371 (2002).

[8] S. Hahn, F. C. Beyer, A. Gällström, P. Carlsson, A. Henry, B. Magnusson, J. R. Niklas, and E. Janzén, Mater. Sci. Forum **600-603**, 405 (2009).

[9] S. Schmerler, T. Hahn, S. Hahn, J. R. Niklas, and B. Gründig-Wendrock, J. Mater. Sci. Mater. Electron. **19**, 328 (2008).

[10] J. M. Dorkel and J. P. Leturcq, Solid State Electron. **24**, 821 (1981).

[11] N. Schüler, T. Hahn, S. Schmerler, S. Hahn, K. Dornich, and J. R. Niklas, J. Appl. Phys. **107**, 064901 (2010).

[12] J. A. Hornbeck and J. R. Haynes, Phys. Rev. **97**, 311 (1955).

[13] N. Schüler, T. Hahn, K. Dornich, and J. R. Niklas, Solid State Phenomen. **156-158**, 241, (2010).

[14] K. Bothe, R. Sinton, and J. Schmidt, Prog. Photovolt. Res. Appl. **13**, 287 (2005).

[15] H. Habenicht, M. C. Schubert, and W. Warta, J. Appl. Phys. **108**, 034909 (2010).

[16] K. Dornich, K. Niemietz, M. Wagner, and J. R. Niklas, Mater. Sci. Semicond. Proc. **9**, 241 (2006).

[17] A. Borghesi, B. Pivac, A. Sassalla, and A. Stella, Appl. Phys. Rev. **9**, 4169 (1995).

[18] K. Niemietz, K. Dornich, M. Ghosh, A. Müller, and J. R. Niklas, Proceedings of the 21st European Photovoltaic Solar Energy Conference, Dresden, Germany, 2006, pp. 361–364.

[19] B. Gründig-Wendrock, K. Dornich, T. Hahn, U. Kretzner, and J. R. Niklas, Eur. J. Appl. Phys. **27**(1–3), 363 (2004).

[20] K. Mojeiko-Kotlinska, H. Scibior, I. Brylowska, and M. Subotowicz, Phys. Status Solidi A **138**, 217 (1993).

[21] S.-K. Min, E. K. Kim, and H. Y. Cho, J. Appl. Phys. **63**, 4422 (1988).

[22] S. Hahn, K. Dornich, T. Hahn, A. Köhler, and J. R. Niklas, Mater. Res. Soc. Symp. Proc. **9**, 355 (2005).

[23] S. Hahn, K. Dornich, T. Hahn, B. Gründig-Wendrock, B. Schwesig, G. Müller, and J. R. Niklas, Proceedings of the MRS Spring Meeting, San Francisco, USA, 2005, pp. 573–578.

[24] A. A. Lebedev, Semiconductors **33**, 107 (1997).

[25] C. G. Hemmingsson, N. T. Son, and E. Janzén, Appl. Phys. Lett. **74**, 839 (1999).

[26] W. Suttrop, G. Pensel, and P. Lanig, Appl. Phys. A **51**, 231 (1990).

Manuscript No.

Author/Title/Issue No.

Please correct your galley proofs and return them within 4 days together with the completed reprint order form. The editors reserve the right to publish your article with editors' corrections if your proofs do not arrive in time.

After having received your corrections, your paper will be published online up to several weeks ahead of the print edition in the EarlyView service of Wiley Online Library (wileyonlinelibrary.com).
Please keep in mind that reading proofs is your responsibility. Corrections should therefore be clear. The use of standard proof correction marks is recommended. Corrections listed in an electronic file should be sorted by line numbers.
LaTeX and Word files are sometimes slightly modified by the production department to follow general presentation rules of the journal.

Note that the quality of the halftone figures is not as high as the final version that will appear in the issue.

Check the enclosed galley proofs very carefully, paying particular attention to the formulas (including line breakings introduced in production), figures, numerical values, tabulated data and layout of the pages.
A black box (■) or a question at the end of the paper (after the references) signals unclear or missing information that specifically requires **your attention.** Note that the author is liable for damages arising from incorrect statements, including misprints.

The main aim of proofreading is to correct errors that may have occurred during the production process, **and not to modify the content of the paper**. Corrections that may lead to a change in the page layout should be avoided.

Note that sending back a corrected **manuscript** file **is of no use**.

If your paper contains **color figures**, please fill in the Color Print Authorization and note the further information given on the following pages. Clearly mark desired **color print figures** in your proof corrections.

Return the corrected proofs within 4 days by e-mail.

Please do not send your corrections to the typesetter but to the Editorial Office:

E-MAIL: pssa.proofs@wiley-vch.de

Please limit corrections to errors in the text; cost incurred for any further changes or additions will be charged to the author, unless such changes have been agreed upon by the editor.

Full color reprints, PDF files, Issues, Color Print, and Cover Posters may be ordered by filling out the accompanying form.

Contact the Editorial Office for **special offers** such as

- Personalized and customized reprints (e.g. with special cover, selected or all your articles published in Wiley-VCH journals)
- Cover/frontispiece publications and posters (standard or customized)
- Promotional packages accompanying your publication

Visit the **MaterialsViews.com Online Store** for a wide selection of posters, logos, prints and souvenirs from our top physics and materials science journals at www.cafepress.com/materialsviews

Order Form

WILEY Publishers Since 1807

physica status solidi a
www.pss-a.com
applications and materials science

2011

WILEY-BLACKWELL
WILEY-VCH GmbH & Co. KGaA
physica status solidi
Rotherstrasse 21
0245 Berlin
Germany
TEL 0 0433
FAX 0 0433
EMAL pssa.proofs@wiley-vch.de

Manuscript No. _____

Author/Title/Issue No.

_____

_____

Please complete this form and return it by FAX or e-mail.

Required Fields may be filled in using Acrobat Reader

Reprints/Issues/PDF Files/Posters

Whole issues, reprints and PDF files (300 dpi) for an unlimited number of printouts are available at the rates given on the third page. Reprints and PDF files can be ordered before *and after* publication of an article. All reprints will be delivered in full color, regardless of black/white printing in the journal.

Reprints

Please send me and bill me for

☐ full color reprints with color cover

☐ full color reprints with color cover *and* customized color sheet

Issues

Please send me and bill me for

☐ entire issues

PDF

Please send me and bill me for

☐ a PDF file (300 dpi) for an unlimited number of printouts **with customized cover sheet.**

The PDF file will be sent to your e-mail address.

Send PDF file to: _____

Please note that posting of the final published version on the open internet is not permitted. For author rights and re-use options, see the Copyright Transfer Agreement at http://www.wiley.com/go/ctavchglobal.

Cover Posters

Posters are available of all the published covers in two sizes (see attached price list). **Please send me and bill me for**

☐ A2 (42 × 60 cm/17 × 24in) posters

☐ A1 (60 × 84 cm/24 × 33in) posters

Mail reprints and/or issues and/or posters to (no P.O. Boxes):

_____

Color print authorization

Please bill me for

☐ color print figures (total number of color figures)

☐ YES, please print Figs. No. _____ in color.

☐ NO, please print all color figures in black/white.

VAT number: _____

Tax-free charging can only be processed with the **VAT** number of the institute/company. To prevent delays, please provide us with the VAT number with this order.

Purchase Order No.: _____

Terms of payment:
☐ Please send an invoice   ☐ Cheque is enclosed
Please charge my credit card

VISA ☐   MasterCard ☐   AMERICAN EXPRESS ☐

Expiry date _____

Card no.	
Card Verification Code	

Date, Signature _____

Send bill to:

_____

Signature _____

Date _____

Subscriptions

For ordering information, claims and any enquiry concerning your journal subscription please go to www.wileycustomerhelp.com or contact your nearest office.
Americas: e-mail: cs-journals@wiley.com; Tel: +1 781 388 8598 or +1 800 835 6770 (toll free in the USA & Canada)
Europe, Middle East and Africa: e-mail: cs-journals@wiley.com; Tel: +44 (0) 1865 778315.
Asia Pacific: e-mail: cs-journals@wiley.com; Tel: +65 6511 8000.
Japan: For Japanese speaking support, e-mail: cs-japan@wiley.com; Tel: +65 6511 8010 or Tel (toll-free): 005 316 50 480.

Price List for Reprints 2011 – pss (a)

The prices listed below are valid only for orders received in the course of 2011. Minimum order is 50 copies.
Reprints can be ordered before *and after* publication of an article. All reprints are delivered with color cover and color figures. If more than 500 copies are ordered, special prices are available upon request.
Single issues are available to authors at a reduced price.
The prices include mailing and handling charges. All prices are subject to local VAT/sales tax.

Reprints with color cover	Price for orders of (in Euro)					
Size (pages)	50 copies	100 copies	150 copies	200 copies	300 copies	500 copies*
1– 4	330,—	385,—	425,—	445,—	548,—	752,—
5– 8	470,—	556,—	608,—	636,—	784,—	1077,—
9–12	610,—	717,—	786,—	824,—	1016,—	1396,—
13–16	744,—	874,—	958,—	1004,—	1237,—	1701,—
17–20	885,—	1040,—	1138,—	1196,—	1489,—	2022,—
for every additional 4 pages	140,—	164,—	175,—	188,—	231,—	315,—
for additional customized colored cover sheet	**190,—**	**340,—**	**440,—**	**650,—**	**840,—**	**990,—**

PDF file (300 dpi, unlimited number of printouts, customized cover sheet) € 330.00

Issues € 48.00 per copy for up to 10 copies.*

Cover Posters • A2 (42×60 cm/17×24in) € 49.00
• A1 (60×84 cm/24×33in) € 69.00

*Prices for more copies available on request.

> **Special offer: If you order 100 or more reprints you will receive a pdf file (300 dpi, unlimited number of printouts, color figures) and an issue for free.**

Color figures

If your paper contains **color figures**, please notice that, generally, these figures will appear in color in the online PDF version and all reprints of your article at no cost. This will be indicated by a note „(online color at: www.pss-a.com)" in the caption. The print version of the figures in the journal hardcopy will be black/white unless the author explicitly requests a color print publication and contributes to the additional printing costs.

	Approximate color print figure charges
First figure	€ 495.00
Each additional figure	€ 395.00 Special prices for more color print figures on request

If you wish color figures in print, please answer the **color print authorization** questions on the second page of our Order Form and clearly mark the desired color print figures in your proof corrections.

Information regarding VAT:

Please note that for German sales tax purposes the charge for *color print* is considered a service and therefore is subject to German sales tax. For **institutional** customers in other countries the tax will be waived, i.e. the Recipient of Service is liable for VAT. Members of the EU will have to present a VAT identification number. Customers in other countries may also be asked to provide according tax identification information.